Influence of texture in hybrid carbon-phosphomolybdic acid materials on their performance as electrodes in supercapacitors

Pablo Palomino [a, *], Jullieth Suarez-Guevara [b], Mara Olivares-Marín [c], Vanesa Ruiz[b, 1], Deepak P. Dubal [b], Pedro Gomez-Romero[b], Dino Tonti [c], Eduardo Enciso [a]

a) Departamento de Química Física I, Facultad de Ciencias Químicas, Universidad Complutense de Madrid (UCM), Avenida Complutense s/n, ES 28040. Madrid, Spain

b) Catalan Institute of Nanoscience and Nanotechnology (ICN2), CSIC and the Barcelona Institute of Science and Technology, Campus UAB, Bellaterra 08193, Barcelona, Spain

c) Institut de Ciència de Materials de Barcelona-Consejo Superior de Investigaciones Científicas (ICMAB-CSIC), Campus de la UAB, E-08193 Bellaterra, Barcelona, Spain

1) Current address: European Commission, Joint Research Centre, Institute for Energy and Transport (IET), Rue du Champ du Mars/Marsveldtstraat 21, 1050 Brussels, Belgium.

E-mail address: Ppalomino@ucm.es (P. Palomino)

ABSTRACT

In this paper, phosphomolybdic acid $H_3PMo_{12}O_{40}$ (PMo_{12}) was anchored to four synthetic micro- mesoporous carbons and a commercial one to analyse the relationship between the porous texture of the support, the PMo_{12} adsorption and the performance of the resulting hybrid materials as electrodes in supercapacitors. The uptake of PMo_{12} on carbon supports follows a clear correlation with the micropore volume, which implies that PMo_{12} is mainly adsorbed in microporosity as a consequence of a greater confinement in this kind of pores instead of mesopores. Transmission electron microscopy indicates that the PMo_{12} adsorbed is homogeneously dispersed in the carbon texture. Finally, the addition of PMo_{12} to the original carbon electrodes provided capacitances up to 293 F per gram of electrode, substantially larger than the 206-240 F g^{-1} of the unmodified activated carbon. This result represented an increase of up to 35% in terms of gravimetric energy density and 160% in terms of volumetric energy density, after PMo_{12} integration into the carbon matrix.

1. Introduction

The depletion of fossil fuels and concerns about climate change are leading towards a new and sustainable model of generation and management of energy [1], promoting the use of sustainable energy sources to satisfy our energy demand [2]. This urgent need to improve efficiency and sustainability of the current energy model has turned electrical energy storage into an issue of great importance, thus boosting research on new energy storage systems and on the improvement of existing ones [3].

In this context, supercapacitors, also called electrochemical capacitors, appear as a real alternative in the electrochemical energy storage field [4] capable of meeting some specific requirements of high-power energy applications such as hybrid electric vehicles or other electric appliances. There are two main types of super- capacitors [5]: (i) Double-Layer Capacitors based on the electro- physical mechanism derived from charge polarization at the electric double layer and (ii) Pseudocapacitors based on certain redox processes taking place al variable potentials energy [1].

Porous carbon materials belong to the first type and feature large surfaces that favour energy storage at the double layer. Transition metal oxides and conducting polymers belong to the second type since they may undergo faradaic processes allowing for redox charge storage; making them all fundamental candidates for supercapacitor electrode materials [4]. Specifically, carbon materials have been playing a significant role in the development of alternative clean and sustainable energy technologies due to their good conductivity, high surface area, controlled bulk and surface chemistry, tunable porous structure, low cost, and availability [6,7]. On the other hand, their energy storage mechanism (electric double layer) limits their energy density. Therefore, methods to enhance the electrochemical performance of these carbon materials have been widely investigated by incorporating other materials such as conducting polymers or metal oxides, which present a significant high redox activity [1].

Metal oxides, represent an attractive alternative as electrode materials for supercapacitors due to their high gravimetric capacitance, which results in devices of

high energy and power density. Among the available metal oxides, hydrated RuO_2 has been one of the most studied due to its good performance [8], but it is too expensive for practical application. Other oxides, such as MnO_2, Co_3O_4, NiO, Fe_3O_4, or V_2O_5 have been proposed [9], but most of them are poor electronic conductors [10,11], which does not allow to reach the theoretical capacitances of these metal oxides, limiting the rate capability for high power performance.

Alternatively, a whole family of molecular metal oxide clusters known as polyoxometalates (POMs), are arising great interest in the field of energy storage systems as faradaic electrode materials. Indeed, POMs are nanometric clusters of vanadium, molybdenum or tungsten oxides with well-defined molecular structures with reversible redox activity [12,13]. These clusters were initially pro- posed by our group combined with conducting organic polymers [14e17] and subsequently with carbon materials [18e20] as building blocks for energy storage applications, and in particular for supercapacitors.

The choice of POMs to introduce faradaic processes in the car- bon matrices was based on their higher reversibility, compared to other metal oxides, and their nanometric size (1 nm) resulting in the greatest degree of dispersion [21]. These dispersed nano- particulate electroactive clusters provide maximal active surface, faster electrode reactions and reversible multielectron electro- chemical activity [22], as required in the case of electrochemical supercapacitors.

Since carbon substrates showed a strong affinity for POMs [18, 23, 24], a growing number of papers studying hybrid materials composed of POMs and carbon materials as matrices have been reported, aiming at the development of electrode materials and energy storage devices with improved power and energy densities. Despite these increasing interest on this type of hybrid materials, only a very few examples made with POMs and carbon supports can be found to date. Among the carbon substrates available to produce these composites, carbon nanotubes [25e29], and graphene [20, 30e32] are the most popular matrices to fabricate carbon-POMs electrodes.

On the other hand, activated carbon have not had the same success on this topic despite patented methods to anchor POMs onto activated carbon were known many years ago [33]. Since only few recent work had been reported on the application of polyoxometalate-activated carbon system as active materials in supercapacitors, our group explored the study of these composites materials and its electrochemical performance during the last years [18,19]. The results showed that adsorbed POMs on activated car- bons supports allows enhancing the performance of the hybrid electrode. Thereby they achieve to combine the double-layer capacitance of the carbon and the redox activity of the metallic oxide, leading to a higher energy and power, as well as much improved cycling stability.

Taking into account all these considerations, we have developed materials composed of a porous carbon matrix with POMs, where a synthetic carbon and three activated carbons derived from it as well as a commercial one (Norit) were used to support PMo_{12}. The purpose was to study the influence of the carbon texture on the adsorption of PMo_{12} trying to analyse where and how they are adsorbed, and the further use of these hybrid materials as electrodes in supercapacitors.

2. Experimental

2.1. Materials

The original starting carbon material was prepared following the procedure of resorcinol-formaldehyde polycondensation, described originally by Pekala [34], with some modifications. To that effect, resorcinol (R) was diluted in deionized water (W) in a molar ratio R/W of 0.04, and then NaOH solution was added as catalyst (C) being the R/C molar ratio of 250. The mixture was stirred for 30 min. Formaldehyde was then added at a molar ratio R/ F ¼ 0.5, and after 10 min stirring the samples were introduced sealed in an oven at 84 ^{0}C for 72 h. The resulting wet resin was dried for two days at 80 ^{0}C at ambient pressure and then carbonized to obtain the starting carbon. This carbonization was carried out in a horizontal tubular furnace

under a flowing nitrogen atmosphere at 900 ^{0}C for 1 h after a temperature ramp of 3 ^{0}C min^{-1}. Then the sample was allowed to cool down to room temperature under a constant nitrogen flow rate, obtaining a carbon monolith.

In addition to this carbon, three activated carbons were produced through chemical activation from the latter. Activation of the resorcinol-formaldehyde hydrogel obtained in the previous step allowed increasing porosity and porous surface [35,36]. This activation process consisted in the carbonization of the material in the presence of KOH. Specifically, a known amount of carbon monolith, obtained previously, was physically mixed with KOH in ratios of 0.5:1, 1:1 and 3:1 (w/w). The mixture was then carbonized using a heating rate of 3 ^{0}C min^{-1} up to 900 ^{0}C, followed by a 1 h temperature plateau, under a nitrogen atmosphere. After cooling down, the remaining KOH that did not react was removed by washing the dry product, obtained after the carbonization, with HCl solution. To prevent the an initial vigorous reaction the samples were firstly infiltrated with water under vacuum and subsequently 1 M HCl solution was added during 24 h. After checking that the solution has acidic pH, successive washes with water were carried out until the acid was completely removed.

The final step was the infiltration of the different carbons with phosphomolybdic acid, $H_3PMo_{12}O_{40}$ $6H_2O$ (PMo_{12}) (Sigma-Aldrich) based on the procedure developed by Alcaniz et al. [37] with some modifications. The three activated carbons and one carbon xerogel have been used as supports for PMo_{12} impregnation. For the impregnation, six solutions of PMo_{12} with concentrations of 0.25, 1, 2, 5, 10, y 20 mM were prepared. Then 50 mg of dried carbon were infiltrated with 7 mL of aqueous solutions firstly under vacuum until no bubbles are observed and then for 24 h at room temperature at ambient pressure. Next, the obtained infiltrated carbon was washed with water and dried in a muffle at 100 ^{0}C overnight. The amount of PMo_{12} impregnated was determined by the difference between the

initial weight of AC and the final weight of the impregnated sample.

The resulting electrodes were labelled as C250-x PMo_{12}y, where C250 corresponds to the original R/C ratio of the starting carbon xerogel, x represents the mass ratio of activating agent and carbon (w/w) used and y indicates the initial concentration of the PMo_{12} aqueous solution used to infiltrate the samples.

In order to compare with monolith C250, a powdered commercial activated carbon (AC) DLC Super 30, kindly supplied by Norit Chemicals®, were mixed for 24 h with different concentrations of PMo_{12} solutions (0.25, 0.5, 1, 2, 5, 10 and 20 mM), then washed with deionized water, filtered off and dried in a muffle at 80 ^{0}C. The labelling of this material was Norit-PMo_{12}y, where y has the same meaning as in the C250 series.

2.2. Texture characterization of mesoporous carbons

Texture, porosity and composition of synthetic carbons and the commercial one were analysed by electron microscopy, nitrogen adsorption/desorption and energy dispersive X-rays as described below. The comparative study of the different carbons morphology with regard to hybrid carbons was carried out by transmission electron microscopy (TEM) equipped with energy dispersive X-ray (EDX) for qualitative element analysis. Before examination, the samples were dispersed in anhydrous ethanol and deposited on a holey carbon film supported on a copper grid. TEM micrographs were performed with a JEOL (JEOL 3000F) instrument, operating at 100 keV. Nitrogen adsorption/desorption experiments were per- formed at –196 ^{0} C using a Micromeritics ASAP 2020 equipment. Apparent surface area, S_{BET}, was calculated by employing the BET equation [38,39], which is an estimation that allows to obtain the specific surface area. T-plot method was used to obtain the meso-porous surface (S_{mes}) and the micropore volume (V_{mic}) from the slope and

intercept in the t representation [40,41]. Mesopore vol- ume was calculated by applying Barrett-Joyner-Halenda (BJH) method [42] in the adsorption branch between 1.7 and 300 nm. Total pore volume (V_T) was obtained by Gurvitsch's rule at p/ p0 ¼ 0.99 [41]. In order to calculate micropore size distributions, Non-Local Density Functional Theory (NL-DFT) was employed to analysis the low pressures adsorption isotherms, supposing a slit- shape pore geometry [43]. For isotherms of PMo_{12} adsorption on carbon the Langmuir model was used to calculate saturation capacity (q_{SPMo12}) of PMo_{12} in the micropores [44,45].

2.3. Electrochemical tests

The galvanostatic electrochemical characterization of the material was performed by using a two-electrode Teflon Swagelok® cell in symmetric configuration, and were tested using a Biologic VMP3 potentiostat. When C250 carbon monoliths were studied, cells were composed of binder-free film electrodes previously dried at 100 ^{o} C. These coin-like black carbon monoliths had a typical thickness of 0.75 mm, 10 mm in diameter and a weight of 25e45 mg, depending the activation level. In the case of Norit and Norit-PMo_{12} materials, film-types electrodes were prepared using a 5 wt % of PTFE and a 10 wt % of conductive additive (CSP, Timcal). 1M H_2SO_4 (aq.) was used as electrolyte in all cases. The capacitance (C_{cell}) of the system was obtained applying the following equation: C_{cell} (F) ¼ I $(dV/dt)^{-1}$ to the discharging branch of galvanostatic cycles (discarding the ohmic drop). The specific electrode capaci- tance (C_e) was obtained using the simplified expression C_e (F g^{-1}) ¼ $2C_{cell}/m$, where m is the mass of active material in the lightest electrode. This expression is valid when both electrodes are identical and have the same capacitance. In this case, PMo_{12}, which is component with redox activity, could enhance the charge-storing capacity of just one electrode. Although this amounts to not having an optimally balanced cell, it does not compromise the following results reported below.

3. Results and discussion

3.1. Porous texture characterization of carbon supports

Fig. 1 displays the N_2 adsorption-desorption isotherms obtained at $-196\ ^0C$ for the samples used for PMo_{12} impregnations.

All samples show a remarkable nitrogen uptake at low relative pressures ($p/p_0 < 0.2$) related with a developed microporosity, and a further adsorption at higher relative pressures ($p/p_0 > 0.2$) for the whole C250 series, which is indicative of their mesoporous char- acter. In the case of Norit, the isotherm is parallel to the x axis at $p/p_0 > 0.3$, confirming the absence of mesoporosity and macro- porosity. This indicates that all isotherms are a combination of type I and IV following the IUPAC classification [46]. It can be also observed from the figure that the sharpness of the knee at low relative pressures is high for carbons with low activation level (C250-0, C250-0.5 and C250-1), while for the most activated carbon (C250-3) and Norit a rounder knee could be noticed, denoting the existence of a wider microporosity and a small mesoporosity (3e5 nm). Another important detail is that the slope of the linear section and the hysteresis loop remain almost unchanged. This means that the activation process does not destroy the original mesoporous texture of the carbon xerogel. Table 1 collects the porous texture characterization data derived from the N_2 adsorption isotherms.

Table 1 shows that an increase of the chemical activation level in the starting carbon, led to a higher BET surface and pore volume. Furthermore, this increment of area and volume is mainly due to the development of microporosity. In some cases, especially when the ratio activating agent/carbon is high, there is also an increase of the mesoporosity, because the pores created in the activation ac- quire a large enough size to become mesopores.

3.2. Impregnation results: adsorption isotherms

Fig. 2 displays the PMo_{12} adsorption isotherms in different impregnated carbons, plotting the adsorbed amounts of PMo_{12} versus the equilibrium concentration of the impregnating solution.

In general, we notice that the shape of the isotherms in Fig. 2 is quite close to those of Fig. 1, having an initial pronounced uptake followed by a plateau or a linear adsorption. This behaviour suggests that the process of PMo_{12} adsorption is similar to that of physical adsorption in N_2. For Norit, the absorption process takes place at relatively low concentrations with a closed knee, reaching quickly saturation, which is the same trend as the type-I isotherm of Fig. 1. In the case of carbon derived from phenolic resins, there are some discrepancies. As the small mesopores percentage in- creases (samples C250-1 to C250-3), the knee shape becomes broader as a consequence of the heterogeneity of its porosity as we expect. However, for samples C250-0 to C250e0.5, despite a more or less rounded knee shape, there is no increase in the uptake at high concentrations, which is consistent with the monolayer adsorption of the Langmuir model [44,45].

The high PMo12 uptake achieved, especially for sample C250-3, are quite remarkable, attaining masses that exceed the weight of the original carbon. These high loadings obtained here are of the same order, even greater in some cases, than other results reported using PMo12 and activated carbons as supports [47e49]. As it can be appreciated from the figure, the adsorbed amount in the samples seems to be related to the texture characteristics of the adsorbents, thereby samples with high surfaces and pore volume (C250-1 to C250-3) show a higher PMo12 load, while sample C250-0 is the one that shows the least. In order to establish a closer relationship between the porosity versus the amount of PMo12 adsorbed we have fitted the PMo12 adsorption isotherms to the Langmuir model at low concentrations. After obtaining the saturation adsorption (qSPMo12), we plotted these values versus the pore volume of each sample (Fig. 3). While carbons derived from phenolic resins, activated as well as non-activated, follow the same trend with Vmic, Norit

does not seem to follow the same behaviour. Fig. S1 indicate that Norit have a higher proportion of ultramicropores (d < 0.7 nm) and small supermicropores (below 1 nm), which do not allow the access to PMo12, as it is necessary to have a minimum pore size of at least 0.8e1 nm to host the PMo12 [21, 50]. In Fig. S1 Norit also exhibits a low proportion of pores around 1.2 nm, in comparison with C250-x series, supporting the idea, that this material is less able to accommodate effectively PMo12. The fitting equation of Fig. 3 shows that the value obtained for the intercept is very close to zero and, in fact, it could be considered equal zero because in the absence of microporosity, PMo12 adsorption cannot take place. Regarding the slope, 1.18 mmol/cm3 corresponds to 1.4 nm3 per molecule. Compared with the volume of a sphere of 0.4 nm radius, that corresponds, approximately, to the effective thickness of PMo12, this result in a volume of 0.27 nm3. Whereby, 1.4 nm3 per molecule seems a reasonable value, which implies not only a rather compact packing but also that part of the Vmic (ultramicropores) could also be inaccessible for PMo12.

3.3. Porous texture after PMo12 impregnation

Nitrogen adsorption-desorption isotherms of C250e0.5 and some impregnated derived from this latter (C250-0.5-PMo_{12}) are reported in Fig. 4a and b.

As Fig. 4a shows, the isotherm shape is retained with the adsorption of PMo_{12} in all cases, and the N_2 adsorption decreases after the introduction of PMo_{12} as expected. We also note that the higher the initial concentration of the solution (green diamonds), the lower the nitrogen adsorption, being this effect more pro- nounced at low relative pressures. That confirms that PMo_{12} is filling mainly the micropores.

However, we must take into account that PMo_{12} displays a porosity two orders of magnitude lower in comparison with the studied carbon supports [51]. Considering that PMo_{12} does not show a significant porosity and it also supposes an important part in the whole composition of the impregnated sample (reaching as far as 55% of the total weight) due its high density; there is a non- porous mass on the composite. Hence, the adsorption-desorption isotherms must be expressed

as a function of the original carbon weight of the impregnated sample (Fig. 4b) in order to have a more reliable understanding of where the PMo_{12} is accommodated. After analysing Fig. 4b, it is confirmed that there is still a drop of the adsorption at low pressures but this is more sustained after normalising the original data. In addition, a barely significant meso- pore adsorption is observed. The corresponding textural data are shown in Table 2. We note that these data are normalized to the total sample mass, an appropriate procedure to compare the overall porosity of pristine carbon and infiltrated specimens. In the case of the PMo_{12}-filled samples, normalization to the substrate mass is included in parentheses in Table 2, as this Fig. 4 may be used to infer the most likely sites for PMo_{12} confinement.

The data are normalized to the total sample mass. In the case of PMo_{12}-filled samples, normalization to the substrate mass is included in parentheses.

On the observation of Table 2, it can be concluded that PMo_{12} adsorbs within the micropores preferentially (being the decrease in the V_{mic} larger the higher the amount of the adsorbed PMo_{12}) since mesopore surface scarcely experience modifications. This result is in agreement with those displayed previously in Fig. 2, where the amount of PMo_{12} adsorbed depends basically on the microporosity.

3.4. TEM analysis of PMo12

Fig. 5 shows TEM images of a pristine activated carbon (Fig. 5a) and an impregnated activated carbon (Fig. 5b). TEM analysis of the PMo_{12} anchored in the Norit carbon was studied in previous works [20]. As we showed. previously, these carbons have great ability to accommodate metallic nanoparticles, distributing them uniformly throughout the support [52]. In the case of PMo_{12} showed in Fig. 5 we obtained inorganic PMo_{12} clusters well distributed at molecular level within the activated

carbon support, and we also notice that no agglomeration or nanocrystal production is observed. Despite the rough carbon surface and the consequent contrast, the presence of 1 nm sized dark spots is unambiguously detected in Fig. 5b ruling out the possible growth of PMo_{12} crystals and confirming the homogeneous dispersion of the Keggin clusters in the carbon mate- rial. Similar results with even better contrast resolution were found in previous works making use of flatter graphene as substrate [20, 31]. In addition, the corresponding EDX analysis (shown at the bottom of each figure) confirms the presence of these clusters as characteristic molybdenum peaks present only in the spectrum of the impregnated carbon. The EDX also detects the presence of other elements such as Cu (TEM grid used) and O-C (carbon materials).

3.5. Electrochemical tests

Charge-discharge and cyclic voltammogram profiles of the electrodes in two-electrode symmetric cells are displayed, for a complete electrochemical characterization, in Figs. S2 and S3, respectively.

Charge-discharge curves present a marked deviation of the linearity, for impregnated carbons, which is greater as the PMo_{12} content in the carbon support increases. Such behaviour is observed as a curvature of the representations, at low potentials, especially sharp below 0.2 V. In addition of this increase in pseudocapacitance, it can also be notice a double-layer contribution loss, as the slope of the discharge profiles diminish above 0.3 V the higher the PMo_{12} amount. For instance, in Fig. S2a, discharge curves of non-impregnated carbon C250-0-PMo_{12}-0 and the impregnated one C250-0-PMo_{12}-2 converge between 1 and 0.3 V, almost inter- sect, while from 0.3 to 0 V they diverge.

With regard to cyclic voltammograms, they confirm the existence of faradaic processes, which are noticed, in the impregnated samples, due a distortion of the rectangular shape that characterizes the behaviour of an ideal capacitor. The presence of faradaic peaks occurs in the same potential range (0e0.3 V) than charge- discharge profiles, and it is more or less pronounced depending on the

quantity of polyoxometalate uptake. For example, although it can be appreciated that Norit presents an original doubler layer capacitance (Fig. S3e) lower than C250e0.5, its faradaic peak at 0.2 V is remarkably pronounced, because of its higher uptake of PMo_{12} (Fig. 2).

Fig. 6 displays the capacitance retention versus current density of all hybrid electrodes in comparison with the original carbon material. These capacitance data of the different electrodes studied are collected on the basis of charge-discharge data.

The representation of Fig. 6 shows that all hybrid electrodes, except when used as support the non-activated carbon xerogel (Fig. 6a, C250-0-PMo_{12}-y), have a better performance at low current densities mainly due to the effect of PMo_{12}. We notice that as the current density increases, the curves from activated carbon without PMo_{12} intersects the curves of impregnated carbons having higher capacitance at high current density. This is because, at low current density, the faradaic contribution of PMo_{12} is of great importance while at high density current double layer capacitance becomes more important, since the faradaic processes are more kinetic dependent in comparison with the capacitive ones [53]. Addition- ally, the filling of micropores with PMo_{12} could be hindering the ion access to the electrochemically active area, which translates in an additional impedance. In any case, the improvement introduced by PMo_{12} is still remarkable at practically relevant current densities.

This behaviour was previously reported by our group for other carbon materials [18,19]. Furthermore, the greater the amount of PMo_{12} present in the electrode, the greater the drop in capacitance at high currents. The reason is that the PMo_{12} are incorporated in the microporous zone (d < 2 nm), which plays an important role in the formation of the double layer [54], thereby blocking accessibility of the electrolyte ions.

An overview of the electrochemical analysis carried out by charge-discharge galvanostatic measurements is showed in Fig. 7. The specific capacitance for the different hybrid materials

measured at a current density of 6 mA cm^{-2} are:

The figure shows that, after introducing PMo_{12}, there has been clear improvements in performance in all cases except for the non- activated carbon xerogel. The higher the amount of PMo_{12} uptake in the electrode, the larger the electrode capacitance (except for C250-0-PMo_{12}-y), achieving a capacitance maximum around 25-40% of PMo_{12} (C250-x-PMo_{12}-2 series), that suppose an increase of 1.20-1.35 times the capacitance of the original carbon. We note that this increase is more noticeable for activated carbon than for Norit, as the slope of the representations seems to be higher, being even greater as much activation level has the original carbon.

The major increase is attained for electrode C250-3-PMo_{12}, whose capacitance goes from 212 to 285 F per gram of carbon electrode, which represents an increase of 35%.

However, the non-activated carbon experiment a capacitance loss of 18% with respect to the original carbon, moving from 199 to 163 F per gram of electrode.

Using the specific capacitance of the serial materials C250-x- PMo_{12}-2 (where x: 0.5-1-3), Norit-PMo_{12} and C250-0-PMo_{12}-0, gravimetric energy density and gravimetric power were calculated according to the USABC recommendations [55] as E ¼ 1/2 CV^2 and P ¼ 1/8 V^2/ESR (where ESR is the equivalent series resistance), respectively. The working voltage was 1.0 V. Table 3 summarizes the gravimetric energy density and power obtained for carbon and for hybrid materials in two-electrode symmetric cells, normalized per mass of electrode (carbonþPMo_{12}).

The addition of PMo_{12} in carbon xerogels results in electrodes with gravimetric energy densities from 5.8 W h Kg^{-1} to 10.2 W h Kg^{-1} for the hybrid C250-3-PMo_{12}-2. If we take into ac- count the gravimetric energy density of the original carbons, it means an increase of up to 35%. In terms of volume (volumetric energy density), this increase is even higher, reaching, for C250-3- PMo_{12}-2, 2.6 times the energy of the original carbon; this is because the weight of the PMo_{12} cluster is

very large in comparison with carbon. As regards the power parameters, they do not follow the same trend as energy, thus they diminish in gravimetric terms, maintaining their value per volume of electrode.

4. Conclusions

We present an easy route for production of porous carbon and the further incorporation of PMo_{12} nanoclusters into these sup- ports. The N_2 adsorption-desorption isotherms are similar to PMo_{12} adsorption isotherms in almost all cases, being this adsorption greater the higher the porosity of the carbons supports. The reduction of the N_2 adsorption after the impregnation of the pris- tine carbons is observed mainly at low relative pressure, whereas at high relative pressures this decrease is hardly significant. Considering that the present amount of PMo_{12} in the support follows a linear trend with the V_{mic} of the original carbon and the V_{mic} of carbons decrease with the impregnation of PMo_{12}, we can infer that PMo_{12} is basically adsorbed in microporosity. Furthermore, the result of the electrochemical test showed that the incorporation of PMo_{12} clusters into the carbon structure reinforce the electro- chemical performance by adding faradaic processes. Thus, it is possible to improve up to 35% the gravimetric capacitance and 160% the volumetric capacitance with respect to that non-impregnated sample, making these hybrid materials suitable candidates as electrodes in supercapacitors.

Acknowledgments

Work funded by the Spanish MINECO under grants MAT2012-39199-C02-01 and MAT2012-39199-C02-02, P.P. acknowledges a FPI-UCM fellowship (BE45/10) and J. S.-G. a pre-doctoral JAE-CSIC fellowship. ICN2 acknowledges support of the Spanish MINECO through the Severo Ochoa Centers of Excellence Program under Grant SEV-2013-0295.

Figures and Tables

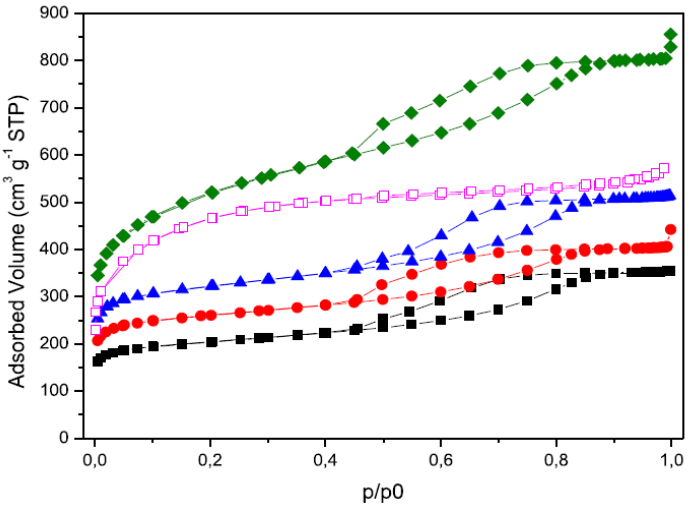

Fig. 1. Adsorption-desorption isotherms of the carbon supports: with different activation level: C250-0 (black solid squares), C250e0.5 (red solid circles), C250-1 (blue solid triangles), C250-3 (green solid diamonds), Norit (purple open squares). (A colour version of this figure can be viewed online.)

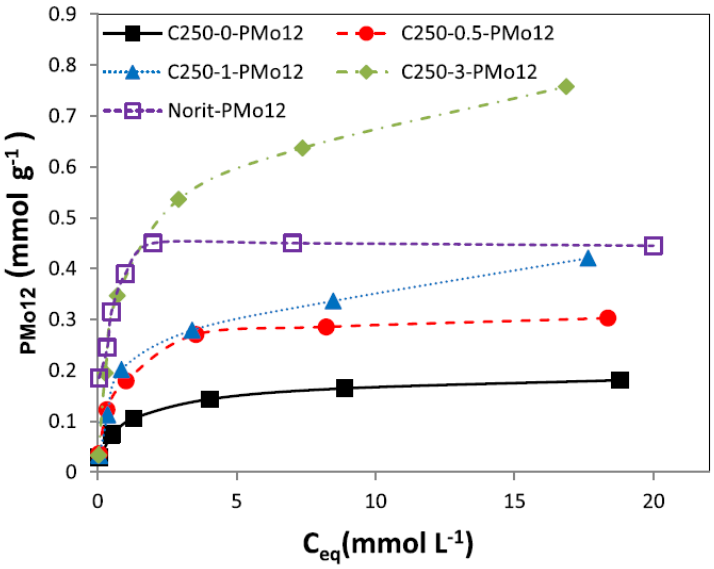

Fig. 2. Representation of the adsorbed amount of PMo12 in mmol per gram of carbon support versus the equilibrium concentration of the impregnating solution: C250-0 (black solid squares), C250e0.5 (red solid circles), C250-1 (blue solid triangles), C250-3 (green solid diamonds), Norit (purple open squares). To guide the eye, lines are inserted. (A colour version of this figure can be viewed online.)

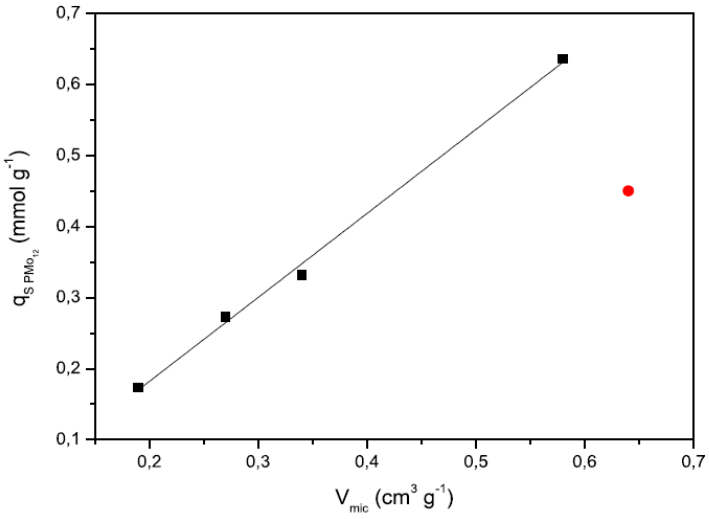

Fig. 3. Representation of q(SPMo12) versus Vmic, Norit carbon is represented as a red diamond. The line represents the fitting equation qSPMo12 = -0.054 + 1.18 Vmic. (A colour version of this figure can be viewed online.)

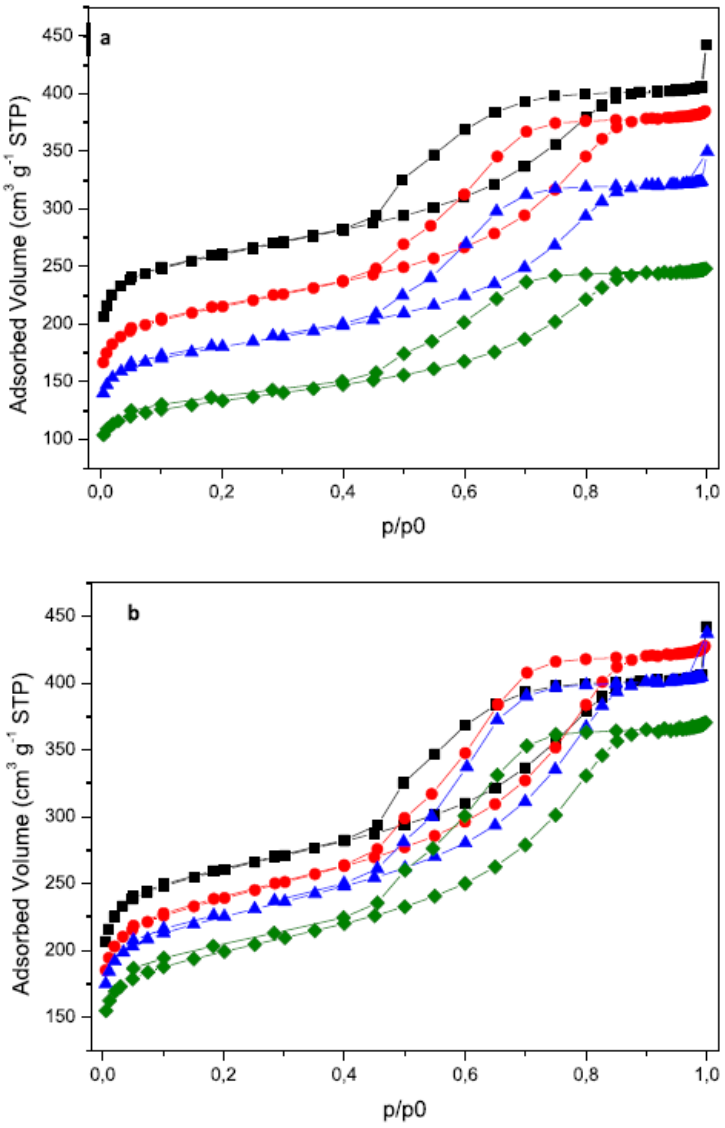

Fig. 4. N2 adsorption-desorption isotherms of the composites derived from C250-0.5 on the basis of total weight (a) and carbon weight (b): PMo12-0 (black squares), PMo12-1 (Red circles), PMo12-2 (Blue triangles) and PMo12-5 (Green diamonds). (A colour version of this figure can be viewed online.)

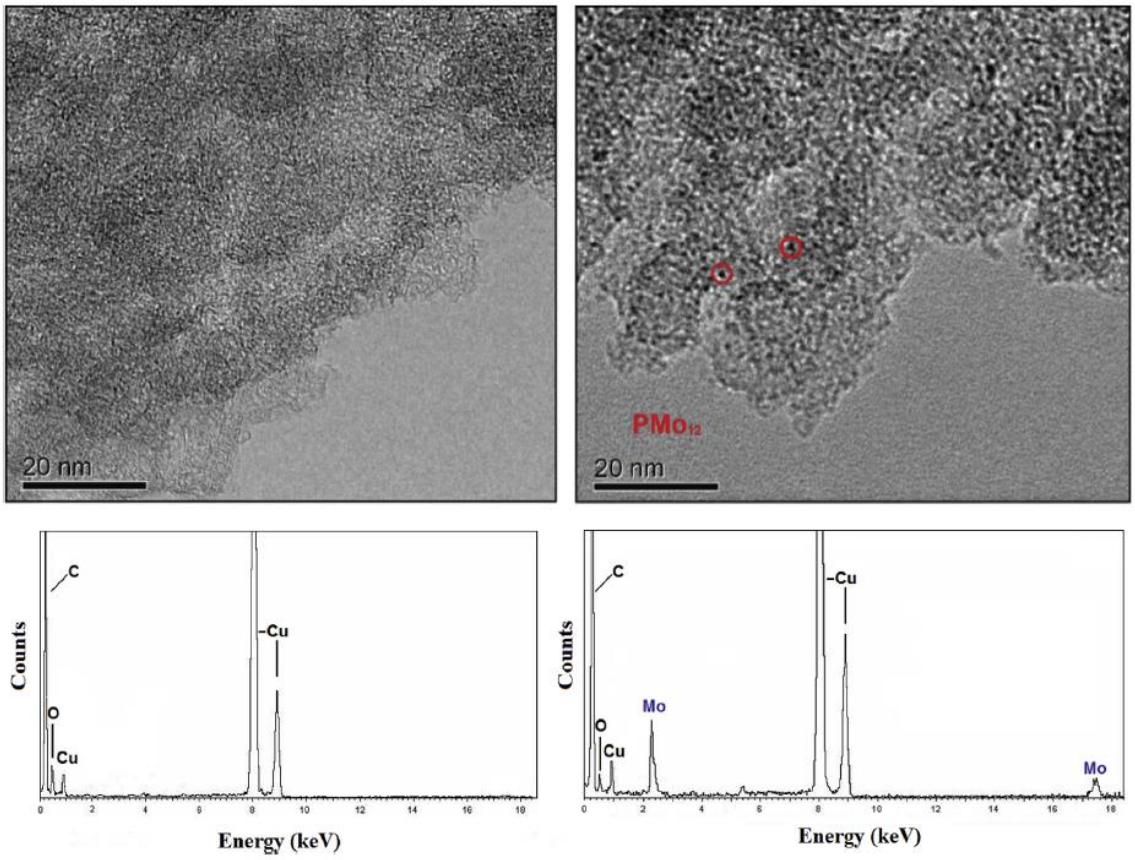

Fig. 5. TEM images of (a) C250-1-PMo12-0 and (b) C250-1-PMo12-5. Bottom insets show EDX spectra of each of the samples. (A colour version of this figure can be viewed online.)

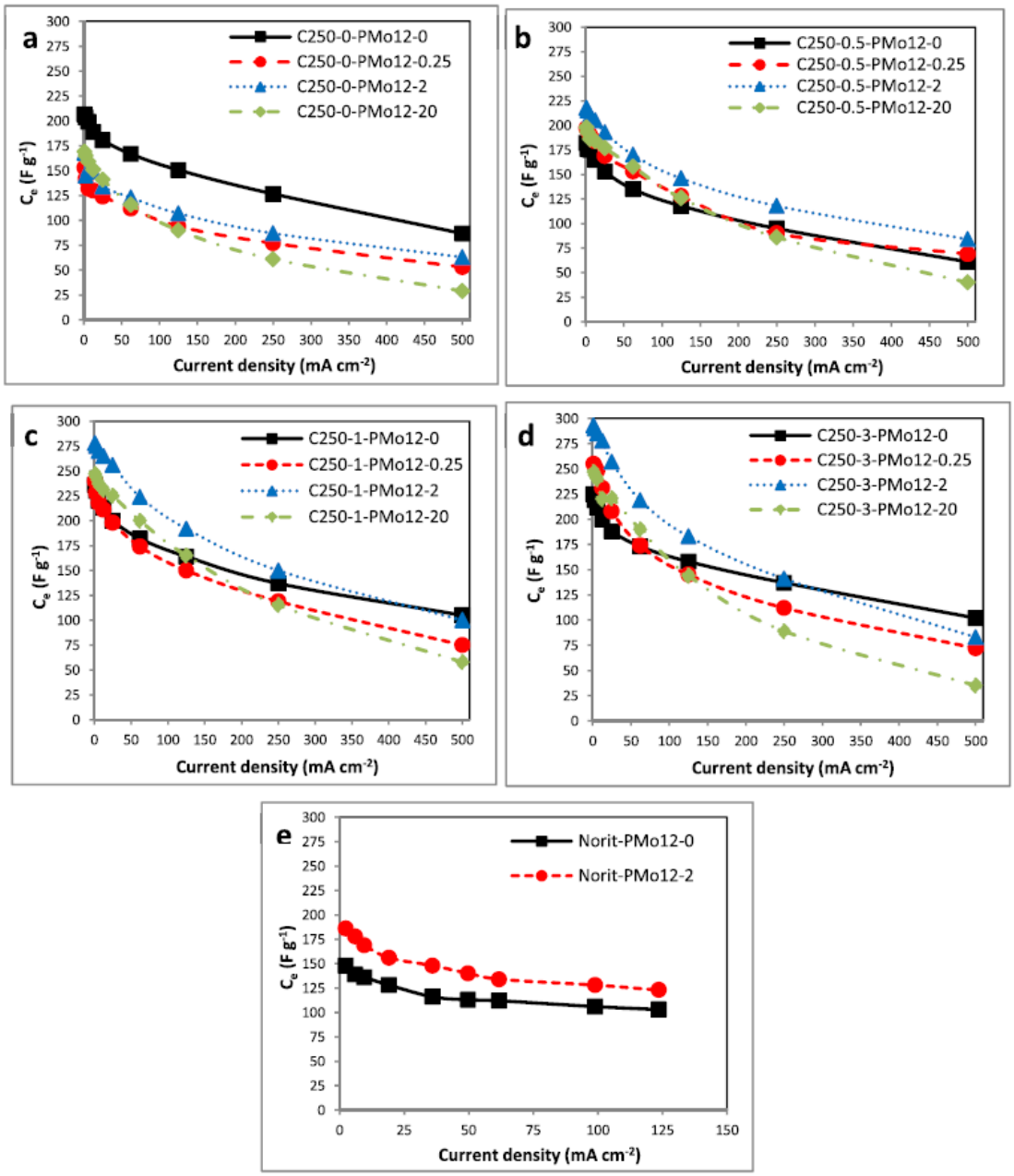

Fig. 6. Specific capacitance of the electrodes per gram of electrode (Ce) as a function of the density current for the hybrid electrodes: a C250-0-PMo12, b C250-0.5-PMo12, c C250-2-PMo12, d C250-3-PMo12, e Norit-PMo12. (A colour version of this figure can be viewed online.)

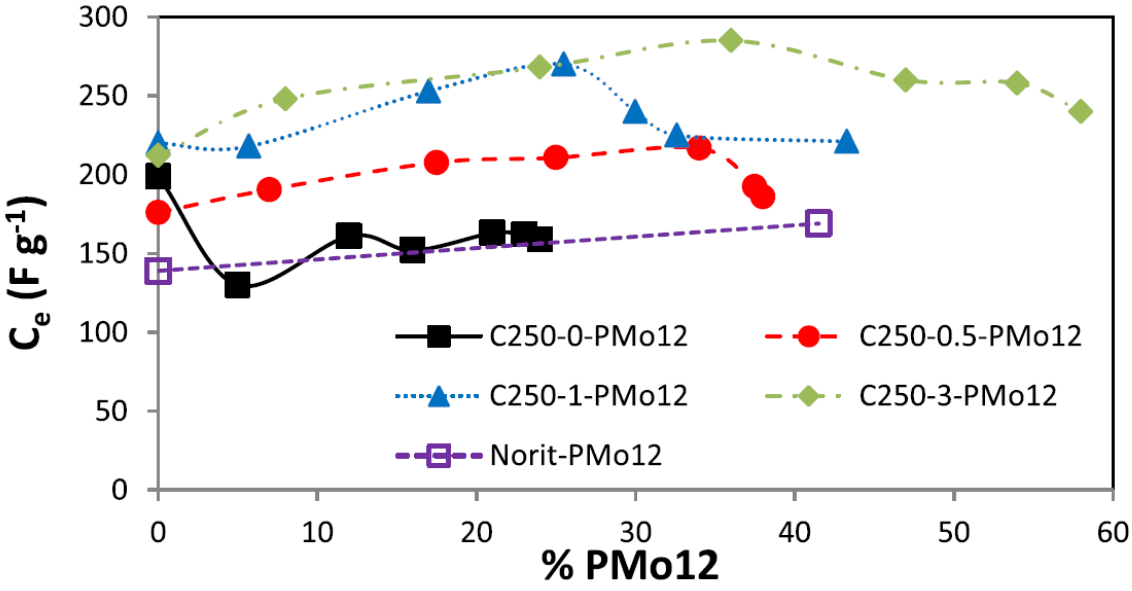

Fig. 7. Specific capacitance per gram of electrode at a current density of 6 mA cm^{-2}. C250-0 (black solid squares), C250e0.5 (red solid circles), C250-1 (blue solid triangles), C250-3 (green solid diamonds), Norit (purple open squares). (A colour version of this figure can be viewed online.)

Table 1
Textural data derived from the N_2 adsorption isotherms of the different supports.

Sample	S_{BET} (m^2 g^{-1})	V_{mic} (cm^3 g^{-1})	S_{mes} (m^2 g^{-1})	V_{mes} (cm^3 g^{-1})	V_t (cm^3 g^{-1})
C250-0	671	0.19	264	0.32	0.55
C250−0.5	853	0.27	288	0.37	0.68
C250-1	1058	0.34	347	0.41	0.79
C250-3	1796	0.58	614	0.72	1.25
Norit	1642	0.64	–	0.24	0.88

Table 2
Textural data of pristine C250−0.5 substrate and PMo_{12}-filled substrates as determined by nitrogen physisorption as a function of the PMo_{12} wt percentage (%PMo_{12}).

Sample	S_{BET} (m^2 g^{-1})	S_{mes} (m^2 g^{-1})	V_{mic} (cm^3 g^{-1})	V_{mes} (cm^3 g^{-1})	%PMo_{12} (wt%)
C250−0.5 PMo_{12}-0	921 (921)	330 (330)	0.28 (0.28)	0.41 (0.41)	0
C250−0.5 PMo_{12}-0.25	857 (920)	316 (339)	0.25 (0.27)	0.41 (0.42)	6.9
C250−0.5 PMo_{12}-1	747 (913)	271 (331)	0.20 (0.24)	0.38 (0.43)	18.2
C250−0.5 PMo_{12}-2	591 (783)	247 (328)	0.15 (0.20)	0.30 (0.40)	24.6
C250−0.5 PMo_{12}-5	441 (658)	218 (325)	0.11 (0.16)	0.24 (0.39)	33.0
C250−0.5 PMo_{12}-10	390 (624)	201 (321)	0.09 (0.14)	0.27 (0.40)	37.5
C250−0.5 PMo_{12}-20	381 (618)	186 (301)	0.09 (0.14)	0.22 (0.36)	38.3

Table 3
Gravimetric and volumetric energy and power densities for hybrid materials expressed per Kg of electrode (specific) and per volume of electrode (density).

Material	Gravimetric energy density (W h Kg^{-1})	Gravimetric power (kW Kg^{-1})	Volumetric energy density (W h L^{-1})	Volumetric power (kW L^{-1})
C250-0-PMo_{12}-2	5.8 (7.2)	8.5 (7.0)	5.8 (5.3)	7.0 (7.0)
C250-0.5-PMo_{12}-2	7.7 (6.3)	11.0 (8.5)	7.2 (4.1)	7.0 (7.0)
C250-1-PMo_{12}-2	9.6 (8.2)	12.0 (9.0)	8.2 (4.6)	7.0 (7.0)
C250-3-PMo_{12}-2	10.2 (7.6)	15.5 (9.5)	9.2 (3.5)	7.0 (7.0)
Norit-PMo_{12}-2	4.3 (5.1)	15.0	1.6 (1.1)	5.5 (5.5)

Gravimetric and volumetric energy and power densities of the original carbons without PMo_{12} are included in parentheses.

References

[1] D.P. Dubal, O. Ayyad, V. Ruiz, P. Gomez-Romero, Hybrid energy storage: the merging of battery and supercapacitor chemistries, Chem. Soc. Rev. 44 (2015) 1777e1790.

[2] D.G. Kwabi, N. Ortiz-Vitoriano, S.S. Freunberger, Y. Chen, N. Imanishi, P.G. Bruce, et al., Materials challenges in rechargeable lithium-air batteries, MRS Bull. 39 (2014) 443e452.

[3] M. Conte, Supercapacitors technical requirements for new applications, Fuel Cells 5 (2010) 806e818.

[4] B.E. Conway, Electrochemical Supercapacitor: Scientific Fundamentals and Technological Applications, Kluwer Academic/Plenum Publishers, New York, 1999, pp. 1e220.

[5] B.E. Conway, V. Birss, J. Wojtowicz, The role and utilization of pseudocapacitance for energy storage by supercapacitors, J. Power Sources 66 (1997) 1e14.

[6] E. Frackowiak, F. B_eguin, Carbon materials for the electrochemical storage of energy in capacitors, Carbon 39 (2001) 937e950.

[7] E.G. Calvo, F. Lufrano, P. Staiti, A. Brigandì, A. Arenillas, J.A. Men_endez, Optimizing the electrochemical performance of aqueous symmetric supercapacitors based on an activated carbon xerogel, J. Power Sources 241 (2013) 776e782.

[8] J.P. Zheng, T.R. Jow, A new charge storage mechanism for electrochemical capacitors, J. Electrochem. Soc. 142 (1995) L6eL8.

[9] G. Wang, L. Zhang, J. Zhang, A review of electrode materials for electrochemical supercapacitors, Chem. Soc. Rev. 41 (2012) 797e828.

[10] W. Xing, F. Li, Z.F. Yan, G.Q. Lu, Synthesis and electrochemical properties of mesoporous nickel oxide, J. Power Sources 134 (2004) 324e330.

[11] S.H. Lee, C.E. Tracy, J.R. Pitts, Effect of nonstoichiometry of nickel oxides on their supercapacitor behavior, Electrochem. Solid State Lett. 7 (2004) A299eA301.

[12] P. Gomez-Romero, N. Casañ-Pastor, Photoredox chemistry in oxide clusters. Photochromic and redox properties of polyoxometalates in connection with analog solid state colloidal systems, J. Phys. Chem. 100 (1996) 12448e12454.

[13] P. Gomez-Romero, Polyoxometalates as photoelectrochemical models for quantum-sized colloidal semiconducting oxides, Solid State Ionics 101e103 (1997) 243e248.

[14] P. Gomez-Romero, M. Chojak, K. Cuentas-Gallegos, J.A. Asensio, P.J. Kulesza, N. Casan-Pastor, et al., Hybrid organic-inorganic nanocomposite materials for application in solid state electrochemical supercapacitors, Electrochem. Commun. 5 (2003) 149e153.

[15] P. G_omez-Romero, K. Cuentas-Gallegos, M. Lira-Cantú, N. Casa~n-Pastor, Hybrid nanocomposite materials for energy storage and conversion applications, J. Mater. Sci. 40 (2005) 1423e1428.

[16] P. Gomez-Romero, O. Ayyad, J. Suarez-Guevara, D. Munoz-Rojas, Hybrid organic-inorganic materials: from child's play to energy applications, J. Solid State Electrochem. 14 (2010) 1939e1945.

[17] J. Vaillant, M. Lira-Cantu, K. Cuentas-Gallegos, N. Casan-Pastor, P. Gomez-Romero, Chemical synthesis of hybrid materials based on PAni and PEDOT with polyoxometalates for electrochemical supercapacitors, Prog. Sol. State Chem. 34 (2006) 147e159.

[18] V. Ruiz, J. Su_arez-Guevara, P. Gomez-Romero, Hybrid electrodes based on polyoxometalate-carbon materials for electrochemical supercapacitors, Electrochem. Comm. 24 (2012) 35e38.

[19] J. Su_arez-Guevara, V. Ruiz, P. Gomez-Romero, Hybrid energy storage: high voltage aqueous supercapacitors based on activated carbon-phosphotungstate hybrid materials, J. Mater. Chem. A 2 (2014) 1014e1021.

[20] J. Suarez-Guevara, V. Ruiz, P. Gomez-Romero, Stable graphene-polyoxometalate nanomaterials for application in hybrid supercapacitors, Phys. Chem. Chem. Phys. 16 (2014) 20411e20414.

[21] G.M. Brown, M.-R. Noe-Spirlet, W.R. Busing, H.A. Levy, Dodecatungstophosphoric acid hexahydrate, (H5O2 þ)3(PW12O40 3-). The true structure of Keggin's 'pentahydrate' from single-crystal X-ray and neutron diffraction data, Acta Crystallogr. Sect. B 33 (1977) 1038e1046.

[22] M. Sadakane, E. Steckhan, Electrochemical properties of polyoxometalates as electrocatalysts, Chem. Rev. 98 (1998) 219e237.

[23] M. Genovese, K. Lian, Polyoxometalate modified inorganic-organic nanocomposite materials for energy storage applications: a review, Sol. State Mater. Sci. 19 (2015) 126e137.

[24] G. Bajwa, M. Genovese, K. Lian, Multilayer polyoxometalates-carbon nanotube composites for electrochemical capacitors, ECS J. Sol. State Sci. Tech. 2 (2013) M3046eM3050.

[25] A. Karina Cuentas-Gallegos, R. Martinez-Rosales, M. Baibarac, P. Gomez-Romero, M.E. Rincon, Electrochemical supercapacitors based on novel hybrid materials made of carbon nanotubes and polyoxometalates, Electrochem. Comm. 9 (2007) 2088e2092.

[26] M. Skunik, M. Chojak, L.A. Rutkowska, P.J. Kulesza, Improved capacitance characteristics during electrochemical charging of carbon nanotubes modified with polyoxometallate monolayers, Electrochim. Acta 53 (2008) 3862e3869.

[27] S. Park, K. Lian, Y. Gogotsi, Pseudocapacitive behavior of carbon nanoparticles modified by phosphomolybdic acid, J. Electrochem. Soc. 156 (2009) A921eA926.

[28] M. Genovese, K. Lian, Pseudocapacitive behavior of Keggin type polyoxometalate mixtures, Electrochem. Comm. 43 (2014) 60e62.

[29] T. Akter, K. Hu, K. Lian, Investigations of multilayer polyoxometalates-modified carbon nanotubes for electrochemical capacitors, Electrochimica Acta 56 (2011) 4966e4971.

[30] X. Huang, X. Qi, F. Boey, H. Zhang, Graphene-based composites, Chem. Soc. Rev. 41 (2012) 666e686.

[31] D.P. Dubal, J. Suarez-Guevara, D. Tonti, E. Enciso, P. Gomez-Romero, A high voltage solid state symmetric supercapacitor based on graphene -polyoxometalate hybrid electrodes with a hydroquinone doped hybrid gel-electrolyte, J. Mater. Chem. A 3 (2015) 23483e23492.

[32] Z. Cui, C.X. Guo, W. Yuan, C.M. Li, In situ synthesized heteropoly acid/polyaniline/graphene nanocomposites to simultaneously boost both double layer and pseudo-capacitance for supercapacitors, Phys. Chem. Chem. Phys. 14 (2012) 12823e12828.

[33] E. A. Cuellar and M. J. Desmond E. A. Cuellar, M. J. Desmond Polyoxometalate modified carbon electrodes and uses therefor US Pat., 4630176A, 1986.

[34] R.W. Pekala, Organic aerogels from the polycondensation of resorcinol with formaldehyde, J. Mater. Sci. 24 (1989) 3221e3227.

[35] E. Raymundo-Pi~nero, K. Kierzek, J. Machnikowski, F. B_eguin, Relationship between the nanoporous texture of activated carbons and their capacitance properties in different electrolytes, Carbon 44 (2006) 2498e2507.

[36] J. Wang, S. Kaskel, KOH activation of carbon-based materials for energy storage, J. Mater. Chem. 22 (2012) 23710e23725.

[37] J. Alca~niz-Monge, G. Trautwein, S. Parres-Esclapez, J.A. Macía-Agullo, Influence of microporosity of activated carbons as a support of polyoxometalates, Micropor. Mesopor. Mater. 115 (2008) 440e446.

[38] S. Brunauer, P.H. Emmett, The use of Van der Waals Adsorption isotherms in determining the surface area of iron synthetic ammonia catalysts, J. Am. Chem. Soc. 57 (1935) 1754e1755.

[39] S. Brunauer, P.H. Emmett, E. Teller, Adsorption of gases in multimolecular layers, J. Am. Chem. Soc. 60 (1935) 309e319.

[40] B.C. Lippens, B.G. Linsen, J.H. De Boer, Studies on pore systems in catalysts I. The adsorption of nitrogen; apparatus and calculation, J. Catal. 3 (1964) 32e37.

[41] S.J. Sing, K.S. Gregg, Adsorption, Surface Area and Porosity, Academic Press, London, 1967. [42] E.P. Barrett, L.G. Joyner, P.P. Halenda, The determination of pore volume and area distributions in porous substances. I. Computations from nitrogen isotherms, J. Am. Chem. Soc. 73 (1951) 373e380.

[43] J.P. Olivier, Modeling physical adsorption on porous and nonporous solids using density functional theory, J. Porous Mat. 2 (1995) 9e17.

[44] I. Langmuir, The constitution and fundamental properties of solids and liquids. Part I. Solids, J. Am. Chem. Soc. 38 (1916) 2221e2295.

[45] I. Langmuir, The adsorption of gases on plane surfaces of glass, mica and platinum, J. Am. Chem. Soc. 40 (1918) 1361e1403.

[46] K.S.W. Sing, D.H. Everett, R.A.W. Haul, L. Moscou, R.A. Pierotti, J. Rouquerol, et al., Reporting physisorption data for gas/solid systems with special reference to the determination of surface area and porosity (Recommendations 1984), Pure Appl. Chem. 57 (1985) 603e619.

[47] M.A. Schwegler, P. Vinke, M. van der Eijk, H. van Bekkum, Activated carbon as a support for heteropolyanion catalysts, Appl. Catal. A Gen. 80 (1992) 41e57.

[48] I.V. Kozhevnikov, A. Sinnema, R.J.J. Jansen, H. van Bekkum, 17O NMR determination of proton sites in solid heteropoly acid H3PW12O40. 31P,29Si and17O NMR, FT-IR and XRD study of H3PW12O40 and H4SiW12O40 supported on carbon, Catal. Lett. 27 (1994) 187e197.

[49] E. Lopez-Salinas, J.G. Hernandez-Cortez, I. Shifter, E. Torres-García, J. Navarrete, A. Gutierrez-Garrillo, et al., Thermal stability of 12-tungstophosphoric acid supported on zirconia, Appl. Catal. A 193 (2000) 215e225.

[50] M.S. Kaba, I.K. Song, D.C. Duncan, C.L. Hill, Mark A. Barteau, Molecular shapes, orientation, and packing of polyoxometalate arrays imaged by scanning tunneling microscopy, Inorg. Chem. 37 (1998) 398e406.

[51] J.B. McMonagle, J.B. Moffat, Pore structures of the monovalent salts of the heteropoly compounds, 12-tungstophosphoric and 12-molybdophosphoric acid Science, J. Colloid Interface Sci. 101 (1984) 479e488.

[52] J. Morere, S. Royuela, G. Asensio, P. Palomino, E. Enciso, C. Pando, A. Cabañas, Deposition of Ni nanoparticles onto porous supports using supercritical CO2: effect of the precursor and reduction methodology, Phil. Trans. R. Soc. A 373 (2015) 20150014.

[53] M. Winter, R.J. Brodd, What are batteries, fuel cells, and supercapacitors? Chem. Rev. 104 (2004) 4245e4270.

[54] E. Frackowiak, Carbon materials for supercapacitor application, Phys. Chem. Chem. Phys. 9 (2007) 1774e1785.

[55] A. Burke, M. Miller, Testing of electrochemical capacitors: capacitance, resistance, energy density, and power capability, Electrochim. Acta 55 (2010) 7538e7548.